Journal Pre-proof

BCL3 couples cancer stem cell enrichment with pancreatic cancer molecular subtypes

Jiaoyu Ai, Sonja M. Wörmann, Kıvanç Görgülü, Mireia Vallespinos, Sladjana Zagorac, Sonia Alcala, Nan Wu, Derya Kabacaoglu, Alexandra Berninger, Diego Navarro, Ezgi Kaya-Aksoy, Dietrich A. Ruess, Katrin J. Ciecielski, Marlena Kowalska, Ekin I. Demir, Güralp O. Ceyhan, Irina Heid, Rickmer Braren, Marc Riemann, Sabrina Schreiner, Samuel Hofmann, Maria Kutschke, Martin Jastroch, Julia Slotta-Huspenina, Alexander Muckenhuber, Anna Melissa Schlitter, Roland M. Schmid, Katja Steiger, Kalliope N. Diakopoulos, Marina Lesina, Bruno Sainz, Jr., Hana Algül

PII: S0016-5085(21)00578-3
DOI: https://doi.org/10.1053/j.gastro.2021.03.051
Reference: YGAST 64243

To appear in: *Gastroenterology*
Accepted Date: 23 March 2021

Please cite this article as: RRH: *Bcl3* deficiency and CSC-ness and PDAC subtypes

BCL3 couples cancer stem cell enrichment with pancreatic cancer molecular subtypes

Jiaoyu Ai[1], Sonja M. Wörmann[1,13*], Kıvanç Görgülü[1*], Mireia Vallespinos[2,3], Sladjana Zagorac[2,4], Sonia Alcala[2,3], Nan Wu[1], Derya Kabacaoglu[1], Alexandra Berninger[1], Diego Navarro[2,3], Ezgi Kaya-Aksoy[1], Dietrich A. Ruess[1,12], Katrin J. Ciecielski[1], Marlena Kowalska[1], Ekin I. Demir[5], Güralp O. Ceyhan[5], Irina Heid[6], Rickmer Braren[6], Marc Riemann[7], Sabrina Schreiner[8], Samuel Hofmann[8], Maria Kutschke[9], Martin Jastroch[9], Julia Slotta-Huspenina[10,11], Alexander Muckenhuber[10,11], Anna Melissa Schlitter[10], Roland M. Schmid[1], Katja Steiger[10], Kalliope N. Diakopoulos[1], Marina Lesina[1], Bruno Sainz, Jr.,[2,3§] and Hana Algül[1§]*

[1]Comprehensive Cancer Center Munich at the Klinikum rechts der Isar (CCCM[TUM]), Technische Universität München, 81675 Munich, Germany; [2]Department of Biochemistry, Autónoma University of Madrid, School of Medicine, Instituto de Investigaciones Biomédicas "Alberto Sols" CSIC-UAM, 28029 Madrid, Spain; [3]Enfermedades Crónicas y Cáncer Area, Instituto Ramón y Cajal de Investigación Sanitaria (IRYCIS), Madrid, Spain; [4]Department of Surgery and Cancer, Division of Cancer, Imperial College London, Imperial Centre for Translational and Experimental Medicine (ICTEM), London, UK; [5]Chirurgische Klinik und Poliklinik, Klinikum rechts der Isar, Technische Universität München, 81675 Munich, Germany; [6]Institute for Diagnostic and Interventional Radiology, Klinikum rechts der Isar der, Technische Universität München, 81675, Munich, Germany; [7]Leibniz Institute on Aging, Fritz Lipmann Institute (FLI), 07745 Jena, Germany; [8]Institute for Virology, Technical University of Munich, 85764 Neuherberg, Germany; [9]Institute for Diabetes and Obesity, Helmholtz Zentrum München, German Research Center for Environmental Health (GmbH), 85748 Munich-Garching, Germany; [10]Institute for Pathology, Technische Universität München, 81675 Munich, Germany; [11]MTBio-biobank of the Technische Universität München and the University Hospital Klinikum rechts der Isar, 81675 Munich, Germany; [12]Medical Center - University of Freiburg, Center for Surgery, Department of General and Visceral Surgery, 79106 Freiburg, Germany; [13]Ahmed Cancer Center for Pancreatic Cancer Research, MD Anderson Cancer Center, University of Texas, Houston, TX 77030, USA

**Jiaoyu Ai, Sonja M. Wörmann and Kıvanç Görgülü contributed equally to this manuscript*
§ Hana Algül and Bruno Sainz share senior authorship.

Short Title: *Bcl3* deficiency and CSC-ness and PDAC subtypes

Grant Support: This work was supported by the Deutsche Forschungsgemeinschaft (Grant AL 1174/4-1, AL1174/4-2 and Collaborative Research Center 1321 “Modeling and Targeting Pancreatic Cancer” to H.A., SFB824 Z2 to K.S.), the Deutsche Krebshilfe (Grant 111646 to H.A.), a Ramon y Cajal Merit Award from the Ministerio de Economía y Competitividad, Spain (to B.S.Jr), a Coordinated Grant from Fundación Asociación Española Contra el Cáncer (GC16173694BARB to B.S.Jr), funding from The Fero Foundation (to B.S.Jr) and a Proyecto de Investigacion de Salud, ISCIII, Spain (no. PI18/00757; to B.S.Jr). Al Jiaoyu is supported by the “China Scholarship Council” grant program.

Abbreviations: PDAC, pancreatic ductal adenocarcinoma; BCL3, B-cell CLL/lymphoma 3; NF-□B,

Nuclear factor-κB; EMT, epithelial to mesenchymal transition; TCA cycle, tricarboxylic acid cycle; SAM, Significance Analysis of Microarrays; OCR, oxygen consumption rate. EUS-FNA, endoscopic ultrasound guided fine needle aspiration.

§ *Corresponding authors:*
Hana Algül, MD, MPH
Comprehensive Cancer Center Munich at the Klinikum rechts der Isar (CCCM^{TUM}),
Technische Universität München, 81675 Munich, Germany
Phone: +49-89-4140-5215
Fax: +49-89-4140-6794
Email: hana.alguel@mri.tum.de

Bruno Sainz, Jr., PhD
Instituto de Investigaciones Biomédicas "Alberto Sols" CSIC-UAM,
28029 Madrid, Spain
Phone: +34-91-497-3385
Fax: +34-91-497-5800
Email: bsainz@iib.uam.es

Conflict of Interest Disclosure Statement: The authors declare no potential conflicts of interest.

Data Availability: ArrayExpress accession number: E-MTAB-3808, E-MTAB-5624; Flow cytometry repository number: FR-FCM-ZY42; GEO accession number: GSE80241

Acknowledgements: We thank the laboratory of Alain Chariot for providing the pcDNA3.1-FLAG-tagged Bcl-3 wildtype plasmid. We thank Christopher Heeschen, during his time at the CNIO, for depositing the RNAseq (E-MTAB-3808) and Methylation (GSE80241) data that was used in this study.

Author Contributions: J.A., S.M.W. and K.G. designed and performed experiments, analyzed data, and prepared the manuscript; M.V., S.Z. and S.A. designed, performed experiments and analyzed the data, N.W., D.K, A.B., D.N., E.K.A., D.A.R., K.J.C. and M.K. analyzed the data and edited the manuscript; E.I.D., C.G. provided human PDAC samples and clinical data, I.H. and R.B. supervised imaging methods, M.R. provided the Bcl3 mouse model, S.S. and S.H. performed the lentivirus transduction, M.K. and M.J. designed experiment and revised the manuscript, J.S.-H., A.M., A.M.S. provided human PDAC histopathological evaluation, K.S. provided histopathological evaluation and helped conceptualization of histopathological approaches, R.M.S, K.N.D, and M.L. revised and edited the manuscript, H.A. and B.S. designed experiments, analyzed data, and revised the manuscript.

ABSTRACT

BACKGROUNG & AIMS: The existence of different subtypes of pancreatic ductal adenocarcinoma (PDAC) and their correlation with patient outcome have shifted the emphasis on patient classification for better decision-making algorithms and personalized therapy. The contribution of mechanisms regulating the cancer stem cell (CSC) population in different subtypes remains unknown.

METHODS: Using RNA-seq, we identified B-cell CLL/lymphoma 3 (BCL3), an atypical NF-□B signaling member, as differing in pancreatic CSCs. To determine the biological consequences of Bcl3 silencing in vivo and in vitro, we generated Bcl3-deficient preclinical mouse models as well as murine cell lines and correlated our findings with human cell lines, PDX models and two independent patient cohorts. We assessed the correlation of BCL3 expression pattern with clinical parameters and subtypes.

RESULTS: BCL3 was significantly downregulated in human CSCs. Recapitulating this phenotype in preclinical mouse models of PDAC via Bcl3 genetic knockout enhanced tumor burden, metastasis, EMT, and reduced overall survival. FACS analyses, together with oxygen consumption, sphere formation, and tumorigenicity assays all indicated that Bcl3 loss resulted in CSC compartment expansion promoting cellular dedifferentiation. Overexpression of BCL3 in human PDXs diminished tumor growth by significantly reducing the CSC population and promoting differentiation. Human PDACs with low BCL3 expression correlated with increased metastasis, and BCL3-negative tumors correlated with lower survival and nonclassical subtypes.

CONCLUSIONS: We demonstrate that Bcl3 impacts pancreatic carcinogenesis by restraining CSC expansion and by curtailing an aggressive and metastatic tumor burden in PDAC across species. Levels of BCL3 expression are a useful stratification marker predicting subtype characterization in PDAC thereby, allowing for personalized therapeutic approaches.

Keywords: pancreatic cancer; metastasis; BCL3; cancer stem cell expansion; PDAC subtypes.

INTRODUCTION

Pancreatic ductal adenocarcinoma (PDAC) is highly lethal and the fourth leading cause of cancer-related death world-wide. By 2030 PDAC is expected to overtake breast and colon cancer mortality in the western hemisphere and become second in line[1]. On the bright side, our growing understanding of the molecular pathology of PDAC has led to a taxonomy classification framework relying on single genetic markers, patterns of genomic alterations, or transcriptional profiles[2-4]. Such subtyping strategies allow for optimization of therapeutic and diagnostic approaches improving overall patient survival. In 2011, PDAC was classified into three subtypes based on transcriptomic data: Classical, Quasi-mesenchymal (QM-PDA), and Exocrine-like[2], refined later on by additional studies[3, 4]. However, a deeper understanding of the molecular patterns defining each subtype is needed. GATA binding protein-6 (GATA6) is augmented in most of progenitor and classical tumors but is absent in basal, squamous, and QM-PDA subtypes[2, 5]. This is biologically relevant as GATA6 is a differentiation marker defining acinar cell maturity and thus influencing tumor progression. The QM-PDA subtype, on the other hand, has been shown to correlate with tumor aggressiveness and poor survival, attributable to tumors with an expanded cancer stem cell (CSC) compartment[6]. Indeed, expansion of CSCs is responsible for the aggressive and inherent chemoresistant nature of tumors[7], yet which factors determine their subclassification in PDAC is not clear.

Nuclear factor-□B (NF-□B) signaling connects inflammation with cancer and can be, activated by the KRAS-pathway. NF-□B regulates PDAC progression in animal models[8 9 10], and promotes stem-like phenotypes in CSCs of different tumor entities[11]. Activated NF-□B signaling can act as both a tumor promoter and a tumor suppressor; however, the specific functional roles of NF-□B family-members in tumor development in general, and in PDAC CSCs specifically, are not well-understood. B-cell CLL/ Lymphoma 3 (BCL3) is an atypical member of the Inhibitor of kappa-B (I□B) family. BCL3 predominantly resides in the nucleus and restrains NF-□B activation via binding to p50 homodimers[12]. Nevertheless, its repressor or activator actions on NF-□B relate to cell types[13]. Animal models of inflammation, including cerulein and sodium taurocholate induced pancreatitis, have associated Bcl3 with inflammatory responses, wherein Bcl3 deficiency provoked disease-severity[14]. In solid tumor formation, BCL3 might also be important as its overexpression has been reported in breast tumors, nasopharyngeal carcinoma, endometrial cancer, and colorectal cancer (CRC)[15]. Additionally, BCL3 is mentioned as a driver of the CSC population in CRC via increasing CRC stem cell markers[16, 17].

Regarding PDAC, *BCL3* was identified as a significantly upregulated gene in patient samples compared to normal tissues by next generation sequencing[18]. Nevertheless, the influence and exact role of BCL3 in pancreatic cancer is not well-understood, especially at the level of CSCs.

In this study, our results illustrate several new aspects of BCL3 in PDAC, CSC biology, and subtype stratification. Using a more clinical setting of endoscopic ultrasound (EUS)-guided fine needle aspiration (FNA), we suggest that BCL3 might also be suitable as a marker for non-classical subtypes of PDAC, thus allowing for better decision-making processes in the clinic.

MATERIALS AND METHOD

Study Approval

All animal procedures were reviewed and approved by the Regierung von Oberbayern, the governmental agency responsible oversight of animal care and use at our institution. In vivo tumorigenicity assays were approved by the Universidad Autonoma de Madrid Ethics Committee (CEI 60-1057-A068) and La Comunidad de Madrid (PROEX 335/14) and in accordance with the guidelines for Ethical Conduct in the Care and Use of Animals as stated in The International Guiding Principles for Biomedical Research involving Animals, developed by the Council for International Organizations of Medical Sciences (CIOMS).

(Supplementary Table 3). *BCL3*-overexpression also lowered overall sphere numbers and sphere forming capacity with no clear difference in the size of spheres over several generations (Figure 1H), suggesting impaired self-renewal. Lastly, *BCL3*-overexpression coincided with increased *GATA6*[20], *PDX1* and *cMYC*, as well as a clear reduction in pluripotency-associated transcripts and *PGC1*□, the latter indicating metabolic reprogramming (Figure 1I).

Bcl3 deficiency influences tumor burden and favors EMT

Next we explored the "BCL3-stemness linkage" *in vivo*, by interbreeding the previously described $Kras^{G12D}$ (*KC*) mouse model of PDAC[21] with *Bcl3*-knockout (termed $Bcl3^{-/-}$)[22] and $p53^{flox/flox}$ (termed $Trp53^{FL}$)[23] mice, obtaining *KCPB* and *KCP* mice. As expected, BCL3 expression was detectable in epithelial tumor cells in *KCP* mice but was ablated in *Bcl3*-deficient *KCPB* mice (Figure 2A). Interestingly, while tumor incidence was unaffected by *Bcl3* expression (100% in both *KCP* and *KCPB*; data not shown), *Bcl3*-deficiency led to significantly enlarged tumors (Figure 2A), as well as significantly reduced overall survival (Figure 2B). Furthermore, in *KCP* and *KCPB* primary tumor-derived cells, where BCL3 protein deletion was confirmed (Supplementary Figure 2A), a cell autonomous *Bcl3*-deficiency-driven acceleration in tumor cell proliferation and colony formation capacity was observed (Supplementary Figures 2B-C). To further study the biological consequences of *Bcl3*-loss in PDAC, 42 *KCP* or *KCPB* tumors were analyzed. In line with our previous findings, a remarkably high incidence of non-classical PDAC subtypes (undifferentiated/anaplastic/sarcomatoid) were observed in *KCPB* compared to *KCP* mice (83% vs. 22%) (Figures 2C-D; Supplementary Table 4). This tendency towards non-classical PDAC subtypes with increased Vimentin (mesenchymal marker) and decreased E-cadherin (epithelial marker) in *KCPB* compared to *KCP* mice was also present at earlier timepoints during pancreatic tumorigenesis (Figure 2E-G). Moreover, the mesenchymal markers Vimentin and Twist were highly expressed over the epithelial markers E-cadherin, □-catenin, and GATA6, an inhibitor of EMT, in *Bcl3*-deficient murine PDAC tumors, indicating *Bcl3*-deficiency-driven EMT (Figure 2H). To validate these findings on a cell-autonomous level, we performed IB (Figure 2I) and immunofluorescence (IF) staining (Supplementary Figure 2D) for Vimentin and E-cadherin in *KCP*- and *KCPB*-derived cell lines. Second, we assessed the expression of EMT factors in *KCP*-derived cells following transient and stable *Bcl3*-knockdown (Supplementary Figure 2E). Third, we examined the expression of EMT factors in *KCPB*-derived cells overexpressing *Bcl3* (Supplementary Figure 2F). All these approaches confirmed a *Bcl3*-deficiency-

driven direct and cell autonomous effect on EMT in PDAC.

Finally, in the less aggressive *KC* mouse model, BCL3 expression was detected by IHC and IBs at each step of PDAC development, including low grade, high grade preneoplastic lesions, PDAC and metastatic foci (Supplementary Figure 2G-H), confirming a role for BCL3 at all steps. However, when isolated *KCB* cells (Supplementary Figure 2 I-J) were orthotopically transplanted into recipient mice, not only were the tumor incidence rates higher and resulting tumors significantly larger, but *KCB*-derived tumors showed increased undifferentiated and sarcomatoid features compared to *KC* cells (Supplementary Figure 2K-M), again confirming that *Bcl3*-loss favors a more aggressive and undifferentiated phenotype.

Bcl3 depletion increases metastatic dissemination of pancreatic cancer cells

The BCL3-EMT link led us to quantify metastatic dissemination, and as expected, *KCPB* mice exhibited significantly increased metastases (Figure 3A). Along the same lines, a direct *Bcl3*-deficiency-driven effect on tumor cell migration (Figure 3B-C), invasion (Figure 3D), and anoikis (Figure 3E) capacity was found *in vitro* in *KCP*-derived cells with stable *Bcl3*-knockdown (Bcl3 shRNA) as well as in primary *KCPB*-derived cells (Supplementary Figures 3A-C). Moreover, NSG mice injected into the tail vein with either *KCP*-derived cells with stable *Bcl3*-knockdown or *KCPB*-derived cells suffered from severe metastatic burden, while mice injected with either *KCP*-derived cells transfected with control (scrambled-shRNA) or non-transfected showed significantly less metastasis (Figures 3F-G; Supplementary Figures 3D-G). Increased metastatic burden was found as early as 7 days post injection with magnetic resonance imaging (MRI) and confirmed by H&E staining (Figure 3F). Late metastases, found in the lung, but also in the liver, were observed and validated by H&E staining (Figure 3G Supplementary Figures 3D-F). Similar results were obtained by bioluminescence imaging of NSG mice injected via the tail vein with either luciferase-labeled *KCPB* or *KCP*-derived cells (Supplementary Figure 3G). Importantly, similar to the primary tumor, an EMT-like phenotype, characterized by Vimentin/Twist expression and E-cadherin/□-catenin downregulation, was observed in the lung metastases developed from *Bcl3*-deficient cells (Supplementary Figure 3H). Thus, for PDAC, *Bcl3*-loss favors EMT and metastasis *in vivo* in a cell autonomous manner.

Bcl3 loss promotes metabolic reprogramming towards oxidative metabolism

To determine how *Bcl3* acts at the cellular level in PDAC, we performed significance analysis of microarray (SAM) on *KCPB*-/*KCP*-derived cells. Strikingly, but consistent with the molecular profile of the QM-subtype, genes linked to metabolic processes, inflammation, cell proliferation, and ECM were increased (Figure 4A), while cell adhesion gene sets, which are highly enriched in the classical subtype, were decreased in the *Bcl3*-deficient subset (Figure 4A). Additionally, microarray analyses revealed that genes related to GATA6 as well as GATA6-levels were significantly decreased in *KCPB*- versus *KCP*-derived cells (Figure 4B, IF staining Figure 4C). Altogether, these data strongly supported a tendency towards a non-classical subtype in *Bcl3* absence. As metabolic processes were the most significantly enriched KEGG pathway gene sets in *Bcl3* absence (Figure 4A), we performed targeted metabolomics. Additionally, to metabolites involved in amino acid metabolism/GSH cycle, *Bcl3* absence significantly elevated TCA cycle/oxidative phosphorylation (OXPHOS)-derived intermediates (Supplementary Figures 4A-B). Furthermore, PGC1α protein in cells and tumor tissues (Figure 4D, Supplementary Figure 4C) as well as mRNA expression levels of mitochondrial biosynthesis markers (*Pgc1*□, *Bnip3*, *Nrf1*, *Nrf2*, and *Nix* (Supplementary Figure 4D)) and mitochondrial/nuclear DNA ratios (Figure 4E) were significantly increased in *Bcl3* absence. Lastly, baseline oxygen consumption rates (OCR), ATP-linked respiration, and maximum OCR were significantly elevated in *KCPB*- versus *KCP*-derived cells (Figure 4F, Supplementary Figure 4E). Taken together, *Bcl3* loss promotes metabolic reprogramming compatible with OXPHOS.

The squamous PDAC subtype or QM-subtype as defined by Collison et al., was characterized by changes in the MYC pathway[4]. Interestingly, Myc target gene sets were significantly reduced in *KCPB*- versus *KCP*-derived cells (Figure 4G), suggesting that *Bcl3*-loss reduces c-Myc signaling. Indeed, a cell autonomous *Bcl3*-deficiency-dependent suppression of c-Myc, specifically the Ser62 phosphorylated "stabilized" form, was confirmed in *KCPB*- versus *KCP*-derived cells (Figure 4H) and in *KCP*-derived cells with transient *Bcl3* siRNA silencing and stable knockdown (Figure 4I-J). Vice versa, increased expression of c-Myc and p-c-Myc was validated in *Bcl3*-overexpressing cells from *KCPB*-derived tumors (Figure 4K-L). Interestingly, among the Myc target genes reduced in *KCPB*-derived cells, members of the miR17-92 cluster displayed significant downregulation (Supplementary Figure 4F). This is of particular interest as we have shown that this cluster is induced by c-Myc and is a negative regulator of PaCSC-ness[24]. Thus and in support of our previously published data [24,25] *Bcl3*-deficiency regulates PaCSCs by suppressing, directly and cell-autonomously, GATA6 and c-Myc expression, ultimately favoring enhanced stem-ness features, metabolic reprogramming, and CSC

enrichment.

Bcl3 affects CSC expansion in murine PDAC cells

As human PaCSCs suppress BCL3 expression, we next evaluated whether Bcl3-loss can expand the CSC-compartment in murine PDAC cells. We observed a significant increase in sphere formation capacity (Figure 5A) and the expression of stem, pluripotency-associated, and EMT gene transcripts (Figure 5B) in KCPB- versus KCP-derived cells. Likewise, Bcl3-loss enriched for CD133+ or CD44+ CSCs in FFPE tumors (Supplementary Figure 5A) and for CXCR4+ expressing cells in digested tumors (Supplementary Figure 5B). Moreover, Bcl3-deficient KCPB cells revealed consistently increased tumor take, enhanced tumorigenicity, greater tumor volumes, and a higher CSC frequency compared to KCP-derived cells (Figure 5C-F), particularly after injection of low cell numbers (5 and 50 cells). Applying the extreme limiting dilution assay (ELDA) algorithm, CSC frequencies were determined to be significantly higher in KCPB- (1/6) compared to KCP-derived cells (1/149) (Figure 5F). Moreover, quantifying highly metastatic $CD133^{+}$/ $CXCR4^{+}$ double-positive population[26] in excised tumors revealed increased percentages in KCPB- versus KCP-derived cells (Figure 5G). Importantly and consistent with our previous findings, the tumors that developed from Bcl3-deficient cells displayed an undifferentiated/ anaplastic phenotype with almost no desmoplastic stroma response (Supplementary Figures 5C-D). Autochthonous tumors from KCPB mice also harbored decreased desmoplastic reaction compared to KCP tumors (Supplementary Figure 5E). Finally, KCPB- compared to KCP-derived cells showed enhanced chemoresistance against gemcitabine (Supplementary Figures 5F), further confirmed in KCP-derived cells following stable Bcl3-knockdown (Supplementary Figures 5G-H). Therefore, key CSC-related features, including tumorigenic potential and elevated CSC markers, correlate with Bcl3 status in murine PDAC cells.

BCL3 overexpression impedes CSC compartment expansion and tumorigenesis

To verify the link between BCL3 and CSC-ness in human PDAC, we further analyzed our PDX-derived BCL3-OE cultures and observed marked reduction in: I) mitochondrial membrane potential and mass (Supplementary Figures 6A-B), II) PDAC chemoresistance (Supplementary Figures 6C-D), and III) importantly, tumor formation and CSC frequency in vivo (Figures 6A-C), indicating that high BCL3 levels antagonize key stem-like properties and/ or decrease the overall CSC pool. Regarding the latter, we observed a marked reduction in CD133/CXCR4-cell percentages from BCL3-OE sphere-

derived cultures (Figure 6D). Likewise, the tumors that developed from *BCL3*-OE cells displayed a more differentiated ductal morphology representing classical subtypes (Figure 6E) and increased GATA6 expression (Figure 6F). Collaterally, a positive transcriptional correlation with *GATA6* and a negative transcriptional correlation with *TGFβ* signaling factors were observed in human samples subjected to supervised hierarchical clustering analysis (Figure 6G). Mechanistically, we observed that by overexpressing *BCL3*, c-MYC and Ser62 p-c-MYC levels were increased and stabilized (Supplementary Figure 6E), resulting in a metabolic gene profile shift from OXPHOS to glycolysis (Supplementary Figures 6F-G and Supplementary Table 5). Therefore, *BCL3*-OE in human PDAC cells affects CSC features, suggesting that low levels of *BCL3* in the PaCSC compartment are necessary for CSC maintenance.

BCL3 is associated with tumor metastases and tumor subtypes in human PDACs

To provide translational relevance and demonstrate a link between BCL3 and clinical parameters/ tumor subtypes, two human PDAC cohorts were probed. BCL3 expression levels vary across human PDACs, as in Cohort-1 (n=66) 71% were classified as BCL3-high, while almost 30% were classified as BCL3-none-low (Figures 7A). Importantly, when PDAC samples were grouped according to BCL3 expression (none-low, high), a significant increase in the incidence of lymph-node metastasis (TILN) in the BCL3 none-low group was found (Figure 7B). However, since Cohort-1 was limited to IB, only a tendency towards distant metastatic capacity driven by BCL3-deficiency could be detected (Figure 7B, Supplementary Table 6). For a more precise validation, we performed an extensive IHC analysis of BCL3 expression for Cohort-2 (n=126). Patients were divided into none/ low/ high BCL3-expressing groups (Figure 7C, Supplementary Table 7), and following stratification distant metastasis was significantly increased in the BCL3 none-low group (Figure 7D). Additionally, we observed decreased survival tendency in the none BCL3-expressing patients compared to low-high BCL3-expressing patients (Supplementary Figure 7A). Moreover, step-wise reduction of BCL3 expression increased TILN (Supplementary Figure 7A). Having observed a link between BCL3 and GATA6 in our murine and human PDX models, we evaluated the utility of combining GATA6 with BCL3. Co-expression examination of BCL3 and *GATA6* by RNA *in situ* hybridization (ISH) in representative human PDACs with BCL3-none-high indeed delineated a positive correlation (Figure 7E). Therefore, we examined the association of BCL3 levels (none, low or high) with specific PDAC subtypes in Cohort-2 via separating them into QM (only KRT81>30% positive)[27,28], exocrine/ADEX (only HNF1A positive)[27,28], mixture of

non-classical subtypes (KRT81/HNF1A positive), and double negative groups representing the classical subtype. First, in BCL3-none PDACs we observed an accumulation of non-classical [single positive (only KRT81 and only HNF1A) and double positive (KRT81/HNF1A positive)] over classical subtypes (double negative) (Supplementary Figure 7B). Focusing on KRT81 expression only as the most stringent marker for the QM-subtype, a negative correlation between the expression levels of BCL3 and KRT81 was observed in representative patients (Figure 7F), and increasing BCL3 expression levels were significantly associated with decreasing KRT81 expression (Figure 7G, Supplementary Figure 7C). A similar, but less pronounced negative association was observed for the exocrine-like subtype and the mixed subtype [both QM and exocrine-like (KRT81>30% positive/HNF1A positive)], with only one high BCL3-expressing patient staining positive for KRT81 (Figure 7H-I, Supplementary Figure 7C, D). To challenge our concept and to strengthen our findings, we stained EUS-guided FNA samples from 2 patients with BCL3, HNF1A, and KRT81 antibodies. This probing showed that high BCL3 levels predicted a classical PDAC subtype for patient #1 (HNF1A-negative, KRT81-negative in EUS-FNA and resected tissue), while low BCL3 expression levels predicted a QM-subtype for patient #2 (HNF1A-negative, KRT81-negative in EUS-FNA and HNF1A-negative, KRT81-positive in resected tissue) (Figure 7J), suggesting that BCL3 indeed helps to stratify PDAC tumors into subtypes.

DISCUSSION

Our data unequivocally reveal new functions for BCL3 in PDAC. *Bcl3*-deficiency in all murine tumor cells resulted in accelerated tumor growth, metastatic dissemination, metabolic switch, and expansion of the CSC compartment *in vivo*, whereas *BCL3*-OE in human PaCSCs severely impeded CSC properties. Interestingly, BCL3 was shown to correlate with GATA6, a surrogate marker for the PDAC classical subtype. Thus, the presence or absence of BCL3 expression can have translational benefit, and we suggest for the first time that BCL3 staining in EUS-guided FNA-samples might enable PDAC-subtyping, thereby allowing for improved decision-making in the clinic.

CSCs from multiple tumor entities mold their phenotype by uniquely overexpressing or repressing mRNAs, miRNAs and/ or proteins[24,25]. By exploiting our published CSC RNAseq and methylome data, we observed that CSCs downregulate a number of genes involved in NF-□B signaling, including *BCL3*. BCL3 is constitutively hyper-phosphorylated at its C-terminal end via GSK3[29,30], regulating turnover and transcriptional activity. Through identification of several BCL3 kinases, a recent study established a convergence of three intertwined signaling pathways in NF-□B activation[31]. Other studies have also described alternate functions for BCL3, such as stabilizing c-MYC by promoting ERK1/2-mediated Ser62-phosphorylation[32]. Likewise, a recent study by Kang et al. showed that the levels of *BCL3* can impair expression of pluripotency-associated genes[33]. In the context of cancer, however, conflicting conclusions regarding the role of BCL3 exist. For example, in CRC, BCL3 has been characterized as a promoter of CSC populations[16] ultimately increasing CRC growth[34], and in breast cancer BCL3 correlated with elevated metastatic behavior and G1 phase transition[35, 36]. Furthermore, BCL3 was assigned to a proto-oncogenic role in leukemia due to its association with mitosis[37]. We, however, show that while BCL3 is expressed in most of PDAC cells, its expression is reduced in the PaCSC compartment. The discrepancies depend on the type of utilized approaches (bulk vs. cell population) and the cancer origin/ background, which will need further exploration for achieving a consensus on BCL3 in cancer and CSCs. We hypothesize that balancing *BCL3* expression in both PDAC cells and PaCSCs represents a mechanism to maintain stemness in "check": (1) when BCL3 levels increase, PaCSCs overexpress c-MYC and down-regulate important stem genes promoting cellular differentiation while maintaining a physiologically-relevant tumor burden, (2) when BCL3 levels remain low, the PaCSC compartment is left "unchecked" and tumor burden/ metastasis dominate. Indeed, we revealed a central CSC suppressor role for *Bcl3*, as *Bcl3* ablation in a murine model of PDAC expanded the CSC pool and significantly accelerated

tumorigenesis and metastasis *in vivo* while over expression of *BCL3* in human PaCSCs impaired key stem properties.

Metabolic alterations have become of major interest with respect to their role in tumor progression, metastasis, and stemness[38]. *Bcl3* can activate metabolism-associated genes and interact with PGC1□, a master regulator of mitochondrial biogenesis, fine-tuning energy homeostasis[39]. In PDAC, *Bcl3* transcriptionally regulates metabolic pathways like glycolysis, limiting oxidative metabolism. Additionally, genes involved in mitochondrial biogenesis (e.g. *Pgc1*□), mitochondrial DNA fraction, and mitochondrial respiration (OCR) consistently increased in *Bcl3* absence, presenting *Bcl3* as a negative regulator of mitochondrial biosynthesis and respiration in PDAC. Having shown that PaCSCs depend on OXPHOS and c-MYC downregulates PGC1□-mediated mitochondrial biogenesis, respiration, and stemness[25], we observed a decrease of c-Myc protein levels and target genes in *Bcl3* absence. At the molecular level, *Bcl3* loss essentially abrogated c-Myc expression and its phosphorylation at Ser62, in line with what has been observed in CRC cells with *Bcl3*-knockdown[32]. Loss of c-Myc allows PGC1□ expression levels to increase, promoting mitochondrial biogenesis, respiration, and metabolic alterations consistent with oxidative metabolism. Indeed, *Bcl3* loss not only promoted OXPHOS, but also enhanced numerous stem-ness features in PDAC cells. Thus, *Bcl3*-deficiency promotes a CSC-like phenotype resulting in “uncontrolled” CSC compartment expansion, accelerated tumorigenesis, and enhanced tumor burden in mice, likely related to the observed OXPHOS enhancement; however, further studies are still required to definitively confirm this association.

Herein we also show that *Bcl3* controls tumor differentiation suppressing an EMT-like phenotype. Mice lacking *Bcl3* exhibited significantly enhanced metastatic burden with a clear mesenchymal over epithelial expression profile, a fact also observed in low *BCL3*-expressing human PDACs. Interestingly, when *BCL3* was overexpressed in human PDX-derived PDAC cells, a clear epithelial over mesenchymal phenotype with increased E-cadherin, cytokeratin and *GATA6* levels resulted. Increased frequency of *GATA6* amplification has been associated with the classical PDAC subtype[5], which in turn defines it as a surrogate marker[2], possessing a pro-epithelial and anti-EMT function in PDAC tumors[20] via both the activation of epithelial genes and the concomitant repression of mesenchymal genes. However, to date, it remains unclear how this transcription factor that binds to the (A/T)GATA(A/G) consensus sequence activating/ repressing gene expression is regulated in PDAC. Our data in human PDXs or in murine PDAC cells suggest a clear link between GATA6 and BCL3. Consistent with this data, we found that most of the non-classical subtypes of PDAC had none-

low levels of BCL3, while the classical subtype tumors exhibited high level of BCL3. Given that GATA6 has been used in the first prospective translational COMPASS study that identifies favorability of broad real time genomic analysis of aggressive PDAC utilizing whole genome and RNA sequencing with a clinically eloquent cycle time, BCL3 might be also used as a predictive marker for non-classical subtypes of PDAC to implement tailored therapeutic approaches for patients.

Our findings related to BCL3, however, challenge previous studies linking characteristics of non-classical subtypes of PDAC in terms of metabolic phenotype[6] and chemotherapy resistance[5]. QM-PDAC tumors display enhanced glycolytic gene expression coining this aggressive subtype as highly glycolytic[40]. Of note, no study has shown the metabolic phenotype of cancer cells isolated from specific PDAC subtypes including the highly glycolytic ones, thus the metabolic profiles at the cellular level of QM-tumors is unknown. Our findings suggest that CSC expansion via BCL3-deficiency leads to metabolic heterogeneity in non-classical subtypes of PDAC by creating dedifferentiated cells and also maintaining continuous stem cell populations. Tumor maintenance by CSCs also mediates gemcitabine resistance contrasting gemcitabine-sensitivity observed in the QM-subtype[2].

In summary, we show that BCL3 represents a CSC repressor and dampens PDAC aggressiveness by restraining the CSC compartment. Moreover, we propose that BCL3 represents a viable candidate for the categorization of PDAC as a non-classical subtype tumor. The expression patterns of BCL3 specifically in PDAC tumors, or within the CSC compartment, might represent an interesting factor whose induction proves clinically beneficial and/ or an interesting tool in translational trials to predict specific PDAC subtypes.

REFERENCES

1. **Siegel RL**, Miller KD, Jemal A. Cancer statistics, 2020. CA Cancer J Clin 2020;70:7-30.
2. **Collisson EA**, **Sadanandam A**, Olson P, et al. Subtypes of pancreatic ductal adenocarcinoma and their differing responses to therapy. Nat Med 2011;17:500-3.
3. **Moffitt RA**, Marayati R, Flate EL, et al. Virtual microdissection identifies distinct tumor- and stroma-specific subtypes of pancreatic ductal adenocarcinoma. Nat Genet 2015;47:1168-78.
4. **Bailey P**, Chang DK, Nones K, et al. Genomic analyses identify molecular subtypes of pancreatic cancer. Nature 2016;531:47-52.
5. **Chan-Seng-Yue M**, **Kim JC**, Wilson GW, et al. Transcription phenotypes of pancreatic cancer are driven by genomic events during tumor evolution. Nat Genet 2020;52:231-240.
6. **Collisson EA**, Bailey P, Chang DK, et al. Molecular subtypes of pancreatic cancer. Nat Rev Gastroenterol Hepatol 2019.
7. **Prasetyanti PR**, Medema JP. Intra-tumor heterogeneity from a cancer stem cell perspective. Mol Cancer 2017;16:41.
8. **Lesina M**, Kurkowski MU, Ludes K, et al. Stat3/Socs3 activation by IL-6 transsignaling promotes progression of pancreatic intraepithelial neoplasia and development of pancreatic cancer. Cancer Cell 2011;19:456-69.
9. **Ling J**, Kang Y, Zhao R, et al. KrasG12D-induced IKK2/beta/NF-kappaB activation by IL-1alpha and p62 feedforward loops is required for development of pancreatic ductal adenocarcinoma. Cancer Cell 2012;21:105-20.
10. **Lesina M**, Wormann SM, Morton J, et al. RelA regulates CXCL1/CXCR2-dependent oncogene-induced senescence in murine Kras-driven pancreatic carcinogenesis. J Clin Invest 2016;126:2919-32.
11. **Rinkenbaugh AL**, Baldwin AS. The NF-kappaB Pathway and Cancer Stem Cells. Cells 2016;5.
12. **Nolan GP**, Fujita T, Bhatia K, Huppi C, Liou HC, Scott ML, Baltimore D. The bcl-3 proto-oncogene encodes a nuclear I kappa B-like molecule that preferentially interacts with NF-kappa B p50 and p52 in a phosphorylation-dependent manner. Molecular and Cellular Biology 1993;13: 3557-3566.
13. **Oeckinghaus A**, Ghosh S. The NF-kappaB family of transcription factors and its regulation. Cold Spring Harb Perspect Biol 2009;1:a000034.
14. **Song L**, **Wormann S**, Ai J, et al. BCL3 Reduces the Sterile Inflammatory Response in Pancreatic and Biliary Tissues. Gastroenterology 2016;150:499-512 e20.
15. **Maldonado V**, Melendez-Zajgla J. Role of Bcl-3 in solid tumors. Mol Cancer 2011;10:152.
16. **Legge DN**, Shephard AP, Collard TJ, et al. BCL-3 promotes a cancer stem cell phenotype by enhancing beta-catenin signalling in colorectal tumour cells. Dis Model Mech 2019;12.
17. **Chen X**, **Wang C**, Jiang Y, et al. Bcl-3 promotes Wnt signaling by maintaining the acetylation of beta-catenin at lysine 49 in colorectal cancer. Signal Transduct Target Ther 2020;5:52.
18. **Liang WS**, Craig DW, Carpten J, et al. Genome-wide characterization of pancreatic adenocarcinoma patients using next generation sequencing. PLoS One 2012;7:e43192.
19. **Salt MB**, Bandyopadhyay S, McCormick F. Epithelial-to-mesenchymal transition rewires the molecular path to PI3K-dependent proliferation. Cancer Discov 2014;4:186-99.
20. **Martinelli P**, Carrillo-de Santa Pau E, Cox T, et al. GATA6 regulates EMT and tumour dissemination, and is a marker of response to adjuvant chemotherapy in pancreatic cancer. Gut 2017;66:1665-1676.
21. **Hingorani SR**, Petricoin EF, Maitra A, et al. Preinvasive and invasive ductal pancreatic cancer and its early detection in the mouse. Cancer Cell 2003;4:437-50.
22. **Riemann M**, Endres R, Liptay S, et al. The IkappaB protein Bcl-3 negatively regulates transcription of the IL-10 gene in macrophages. J Immunol 2005;175:3560-8.
23. **Donehower LA**, **Harvey M**, **Slagle BL**, et al. Mice deficient for p53 are developmentally normal but susceptible to spontaneous tumours. Nature 1992;356:215-21.
24. **Zagorac S**, Alcala S, Fernandez Bayon G, et al. DNMT1 Inhibition Reprograms Pancreatic Cancer Stem Cells via Upregulation of the miR-17-92 Cluster. Cancer research 2016;76:4546-58.
25. **Sancho P**, Burgos-Ramos E, Tavera A, et al. MYC/PGC-1alpha Balance Determines the Metabolic Phenotype and Plasticity of Pancreatic Cancer Stem Cells. Cell Metab 2015;22:590-605.

26. **Hermann PC**, Huber SL, Herrler T, et al. Distinct populations of cancer stem cells determine tumor growth and metastatic activity in human pancreatic cancer. Cell Stem Cell 2007;1:313-23.
27. **Noll EM**, Eisen C, Stenzinger A, et al. CYP3A5 mediates basal and acquired therapy resistance in different subtypes of pancreatic ductal adenocarcinoma. Nat Med 2016;22:278-87.
28. **Muckenhuber A**, Berger AK, Schlitter AM, et al. Pancreatic Ductal Adenocarcinoma Subtyping Using the Biomarkers Hepatocyte Nuclear Factor-1A and Cytokeratin-81 Correlates with Outcome and Treatment Response. Clin Cancer Res 2018;24:351-359.
29. **Bundy DL**, McKeithan TW. Diverse effects of BCL3 phosphorylation on its modulation of NF-kappaB p52 homodimer binding to DNA. J Biol Chem 1997;272:33132-9.
30. **Viatour P**, Merville MP, Bours V, et al. Protein phosphorylation as a key mechanism for the regulation of BCL-3 activity. Cell Cycle 2004;3:1498-501.
31. **Wang VY**, **Li Y**, Kim D, et al. Bcl3 Phosphorylation by Akt, Erk2, and IKK Is Required for Its Transcriptional Activity. Mol Cell 2017;67:484-497 e5.
32. **Liu Z**, **Jiang Y**, **Hou Y**, et al. The IkappaB family member Bcl-3 stabilizes c-Myc in colorectal cancer. J Mol Cell Biol 2013;5:280-2.
33. **Kang S**, Yun J, Kim DY, et al. Adequate concentration of B cell leukemia/lymphoma 3 (Bcl3) is required for pluripotency and self-renewal of mouse embryonic stem cells via downregulation of Nanog transcription. BMB Rep 2018;51:92-97.
34. **Urban BC**, Collard TJ, Eagle CJ, et al. BCL-3 expression promotes colorectal tumorigenesis through activation of AKT signalling. Gut 2016;65:1151-64.
35. **Wakefield A**, Soukupova J, Montagne A, et al. Bcl3 selectively promotes metastasis of ERBB2-driven mammary tumors. Cancer Res 2013;73:745-55.
36. **Westerheide SD**, Mayo MW, Anest V, et al. The putative oncoprotein Bcl-3 induces cyclin D1 to stimulate G(1) transition. Mol Cell Biol 2001;21:8428-36.
37. **Ohno H**, Takimoto G, McKeithan TW. The candidate proto-oncogene bcl-3 is related to genes implicated in cell lineage determination and cell cycle control. Cell 1990;60:991-997.
38. **Peixoto J**, Lima J. Metabolic traits of cancer stem cells. Dis Model Mech 2018;11.
39. **Yang J**, Williams RS, Kelly DP. Bcl3 interacts cooperatively with peroxisome proliferator-activated receptor gamma (PPARgamma) coactivator 1alpha to coactivate nuclear receptors estrogen-related receptor alpha and PPARalpha. Mol Cell Biol 2009;29:4091-102.
40. **Daemen A**, Peterson D, Sahu N, et al. Metabolite profiling stratifies pancreatic ductal adenocarcinomas into subtypes with distinct sensitivities to metabolic inhibitors. Proc Natl Acad Sci U S A 2015;112:E4410-7.

FIGURE LEGENDS

Figure 1. BCL3 is differentially expressed in CSCs of human PDAC. (A) RNA-seq data analysis from PDAC cultures (n=5) grown as either adherent (Non-CSCs/Adh) or anchorage-independent sphere cultures (CSCs/Sph) Top: Gene set enrichment analysis (GSEA) of NF-□B signaling in Non-CSC and CSC isolated from 5-PDX tumors (duplicate samples per PDX). (NES=1.56; FDR q-value=0.014; NOM p-val=0.014). Bottom: Heatmap of NF-□B-related genes in Non-CSC and CSCs groups (one minus Pearson´s correlation). (B) NES scores (obtained by GSEA) for a 19-gene PaCSC signature in human PDAC patients (Bailey dataset) ranked High-to-Low for the 7-NF-□B signaling genes. (*=FDR<0.25). (C) GSEA of 19-gene PaCSC signature in BCL3 low vs. high human PDACs (Bailey dataset). (D) Pearson correlation of BCL3 with average CSC score (Bailey dataset). (E) RT-PCR analysis of relative BCL3 mRNA expression in non-CSCs/Adh and CSC/Sph cultures derived from a panel of 4-human PDAC PDXs. Data were normalized to □-actin. Mean fold changes±SD(n=6) were determined relative to adherent cultures, set to 1.0. (F) Bivariate scatterplots of mRNA expression levels of BCL3 and EMT-related genes from 179-PDAC patients (UCSC-RNAseq database). The EMT score was calculated from the sum of expression of well-known mesenchymal marker genes minus the total expression of known epithelial genes[19] ((FN1+VIM+ZEB1+ZEB2+TWIST1+TWIST2+SNAI1+SNAI2+CDH2)/(CLDN4 +CLDN7+TJP3+MUC1+CDH1)). Pearson's negative correlation of r=-0.28. (G) IF staining of E-cadherin and pan Keratin (PanKRT) in Panc354 cells with a HuBCL3-overexpressing vector and empty vector control. Scale bars=10μm. (H) Representative images and fold-change in sphere formation (mean $n^{spheres}$±SD) of Panc354 cells with a HuBcl3-overexpressing vector compared to empty vector control across first, second and third generations. Empty vector control Panc354 cultures, set to 1.0 (n=3). (I) RT-PCR analysis of relative mRNA expression values of indicated genes in Panc354 cells with a HuBCL3-overexpressing vector compared to empty vector control. Data normalized to □-Actin. Means±SD(n=3). *P<0.05; **P<0.01; ***P<0.001.

Figure 2. Bcl3 deficiency determines tumor burden, dedifferentiation, and favors an EMT. (A)

IHC of Bcl3 in representative pancreata from *KCP* and *KCPB* mice (left). Relative pancreatic weight obtained from *KCP* vs. *KCPB* mice (right). Means±SD(*n*=13). (**B**) Kaplan-Meier survival curve of *KCP* (*n*=27) and *KCPB* (*n* = 27) mice (Median survival *KCP*=69d, *KCPB*=64d). (**C**) H&E staining from representative *KCP* and *KCPB* tumors. (**D**) Pathologist based tumor grading of *KCP* and *KCPB* PDACs. Tumors were divided into two groups: G2/3 and G4 (*n*=42). (**E**) H&E staining of pancreata obtained from representative 4 week-old *KCP* and *KCPB* mice. Normal tissue, ADM and focal tumor formation (ductal/differentiated in *KCP* and undifferentiated/anaplastic/sarcomatoid in *KCPB*) are shown in higher magnification. (**F**) Focal tumor formation percentage per genotype after 4 weeks. (**G**) IHC for E-cadherin and Vimentin in 4 week-old *KCP* and *KCPB* pancreata. (**H**) IHC for Vimentin, Twist, E-Cadherin, □-Catenin and GATA6 in *KCP* and *KCPB* PDACs. (**I**) IB of Vimentin, Twist, E-Cadherin and □-Catenin in representative *KCP* and *KCPB* PDAC tissues. β-Actin is a control. Scale bars=50μm. ***P*<0.01; ****P*<0.001.

Figure 3. Bcl3 regulates metastatic properties in pancreatic cancer. (**A**) H&E stainings and images of lymph-nodes (LN) and liver metastasis (liver) in *KCPB* mice. *KCP* and *KCPB* mice were divided into two groups according to the presence of lymph-node and distant metastases (MET) (*n*=42). (**B**) Migration assay of *KCP*- and *KCPB*-derived cells treated with 1□M cytarabine to eliminate the effect of proliferation during the migratory process. Left: wound closure after 16 hours (h). Right: percentage of wound closure over time. Means±SD(*n*=3). (**C**) Migration assay of *KCP*-derived cells lentivirally-transduced with Bcl3 shRNA or shRNA control and treated with 1□M cytarabine. Left: wound closure after 20h. Right: percentage of wound closure over time. Means±SD(*n*=3). (**D**) Trans-well invasion assay of *KCP*-derived cells lentivirally-transduced with Bcl3 shRNA or shRNA control. Left: Invaded cells visualized after 62h by crystal violet staining. Right: Summary of the percentage of invaded area. Means±SD(*n*=3). (**E**) Anoikis assay of *KCP*-derived cells lentivirally-transduced with Bcl3 shRNA or shRNA control; number of cells undergoing anoikis after 72h were quantified. Means±SD(*n*=3-4 cells/genotype). (**F-G**) Experimental metastasis assay. (**F**) Top: Cranial thoracic MR images with lung metastases (white arrowheads) and H&E staining of the lung from NSG mice, 7d after tail vein injection with *KCP* Bcl3 shRNA or shRNA control transduced cells. Bottom: Metastatic area quantification in the lung. Three H&E slides of 1xmagnification 20□m apart were analyzed per group. Means±SD(*n*=5). (**G**) Top: H&E staining of the lung (left) and liver (right) from NSG mice, 25d after tail vein injection with *KCP* Bcl3 shRNA or shRNA control transduced cells. Bottom: metastatic

amount quantification per field of view (FOV) (left) and metastatic area in the liver (right). Three H&E slides of 1xmagnification 20µm apart were analyzed per group. Means±SD(*n*=5). Scale bars=50µm. **P*<0.05; ***P*<0.01.

Figure 4. Bcl3 loss favors CSC expansion by promoting a metabolic switch towards oxidative metabolism. (A) Microarray based SAM analysis of *KCP* and *KCPB* cells revealed 12-KEGG pathway gene sets to be either >two-fold up/down-regulated in *KCPB* compared with *KCP* cells (Delta=0.46, *n=3*). (B) GSEA microarray data analysis of *KCP- vs. KCPB*-derived cells for GATA6 (NES=1.61; FDR-*q*-value=0.07; NOM ****P*-value=0.000).(*n*=3). (C) IF staining of GATA6 in representative *KCP* and *KCPB* cells. Scale bars=50µm. (D) IB for PGC1α and NPGC1α in *KCPB* vs. *KCP* cells. β-Actin is a control. (E) Mitochondrial/nuclear DNA content ratio in *KCPB*- and *KCP*-derived cells. Means±SD(*n*=3-4). (F) Oxygen consumption rate (OCR) of *KCP*- and *KCPB*-derived cells was measured using the XF Extracellular Flux Analyzer. Tumor cell cultures were subsequently treated by oligomycin (O), FCCP (F), and antimycin+rotenone (A+R) into the culture medium (*n*=3). (G) GSEA microarray data analysis of *KCP- vs. KCPB*-derived cells for c-Myc (NES=1.38; FDR-*q*-value=0.08); NOM ****P*-value=0.000). (*n*=3) (H) IB of c-Myc, p-c-Myc (Ser62) in *KCP*- and *KCPB*-derived cells. (I) IB for Bcl3, c-Myc and p-c-Myc expression in *KCP*-derived cells with Bcl3 siRNA-knockdown. (J) IB of c-Myc and p-c-Myc expression in *KCP*-derived cells with Bcl3 shRNA-knockdown. (K) IB of His-tag, c-Myc and p-cMyc expression in *KCPB*-derived cells with ectopic over-expression of Bcl3 pcDNA4/myc-HisA). β-Actin is a control. (L) RT-PCR analysis of relative c-Myc mRNA expression in *KCPB*-derived cells with ectopic Bcl3-overexpression. Relative fold changes in means±SD(*n*=3) were determined relative to *KCPB*-derived cells, set to 1.0. ***P*<0.01.

Figure 5. Loss of Bcl3 contributes to CSC-ness and CSC-enriched tumor formation in murine PDAC cells. (A) Sphere formation assay in *KCP*- and *KCPB*-derived cells. Representative images and summary of the number (nº) of spheres/ml formed from 5000 input cells. Means±SD(*n*=3-4). (B) *Hes1, Oct3/4, Sox2, Snai1* and *Zeb1* mRNA expression levels were determined by RTqPCR in *KCP*- and *KCPB*-derived cells and normalized to HPRT. Means±SD(*n*=2;6). (C) Mice were subcutaneously (s.c.) injected with the indicated number of *KCP*- and *KCPB*-derived cells resuspended in Matrigel (n=4-8 mice/dilution/group). Summary of in vivo tumor take and growth over 6 weeks. (D-G) 6 weeks post injection, tumors were resected and analyzed. (D) Images of resected tumors, (E) quantification of tumor weights and (F) nº of tumors formed per injection and CSC frequencies determined using the

ELDA algorithm (95%CI). (**G**) Tumors were digested and the percentage of CD133/CXCR4 double-positive cells was determined by flow cytometry. Representative cytometry plots and gating strategy for CD133/CXCR4 positive cells in KCP and KCPB-resected tumors (left). Summary of CD133/CXCR4 cell surface expression in cells isolated from all tumors as indicated (right). Scale bars=50μm. *P<0.05; **P<0.01; ***P<0.001; n.s., not significant.

Figure 6. Overexpression of BCL3 reduces CSC-ness and CSC-enriched tumor formation in PDX-derived cultures. (**A**) Images of harvested tumors from 500 or 50 Panc354 cells with a HuBcl3-overexpressing vector or empty vector control injected into the flanks of nude mice and 10 weeks post injection tumors were resected. (n=4 injections/condition). (**B**) Quantification of tumor weight. Means±SD(n=4). (**C**) Number of tumors formed per injection and CSC frequencies determined using the ELDA algorithm (95%CI). (**D**) Left: Cytometry plots of CD133 or CXCR4 positive cells in BCL3-overexpressing Panc354 spheres determined by flow cytometry. Right: Percentage of CD133/CXCR4 positive cells in Panc354 cells with a HuBcl3-overexpressing vector or empty vector. (n=6). (**E**) H&E staining of tumors obtained after injecting 500 Panc354 cells with a HuBCL3-overexpressing vector or empty vector control into nude mice. **(F)** IHC analysis of GATA6 in tumors obtained after injecting Panc354 cells with a HuBCL3-overexpressing vector or empty vector control into nude mice. Left: Representative pictures of GATA6 IHC. Right: Quantification of GATA6 IHC in tumors. Means±SD(n=4-5). *P<0.05. **(G)** Pearson-correlation matrix of CSC pathway related genes in 179-PDAC patients sorted for BCL3 mRNA levels and nearest neighbor. Scale bars=50μm. *P<0.05; ****P<0.0001.

Figure 7. BCL3 determines tumor metastases, patient survival and tumor subtypes in human PDACs. (A) Cohort-1**.** Left: IB of BCL3 in representative PDAC tissues. ERK2 is control. Right: 66-human PDACs were screened by IB analysis for BCL3. 29% (n=19) failed to express BCL3; 71% (n=47) revealed strong BCL3 expression. **(B)** 48-PDAC patients were screened for BCL3 expression by IB analysis. Up: 17/19 PDACs patients bearing BCL3 negative PDACs suffered from TILN. 30/47 patients with BCL3 positive PDACs were diagnosed with TILN. (n=66; *P<0.05). Down: 2/14 PDACs patients bearing BCL3 negative PDACs suffered from a metastasis. 2/34 patients with BCL3 positive PDACs were diagnosed with metastasis. (n=48; P=0.5695). (**C**) Cohort-2. Representative BCL3 IHC in PDAC tissues separated into none/low/high level expression. **(D)** In Cohort-2, 86/109 PDAC patients with BCL3 none-low suffered from metastasis. 5/9 patients with high BCL3 were metastatic. (n=109,

**P=0.0393*). (E) Representative GATA6 expressions by ISH assay in patients with BCL3-none and BCL3-high. Arrowheads mark GATA6 punctates. (F) Representative BCL3 IHC in PDAC tissues separated into negative (none-low expression) and positive (high expression). KRT81 separated into negative (<30% KRT81-expressing tumors cells) and positive (>30% KRT81-expression tumors cells). Arrowheads mark high-KRT81 and -BCL3-expressing cells. (G) Distinct QM-PDA (KRT81-positive) incidence in 19-patients separated into none(63.2%) vs low(31.6%) vs high(5.2%) BCL3 expression groups. (H) Distinct incidence of Exocrine-like (HNF1A-positive) in 46-patients separated into none(56.5%) vs low(28.3%) vs high(15.2%) BCL3 expression groups. (I) Distinct incidence of double high expression with QM-PDA (KRT81>30%-positive) and Exocrine-like (HNF1A-positive) in 16-patients separated into none(56.25%) vs low(37.5%) vs high BCL3(6.25%) expression groups. (J) Representative patients (#1-#2) with BCL3/HNF1A/KRT81 IHC stainings in FNA and resected tissue samples. Scale bars=50μm.

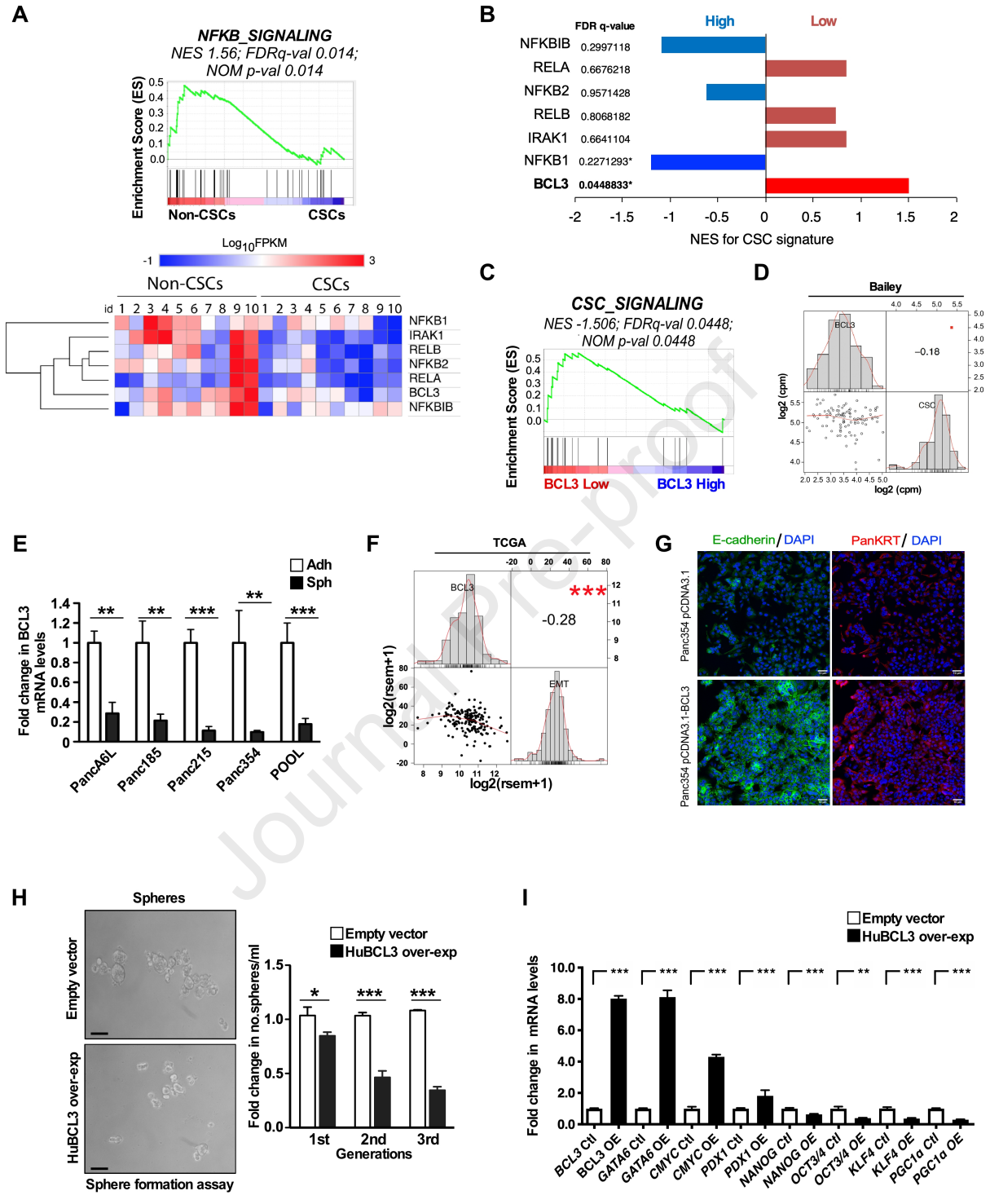

Figure 1

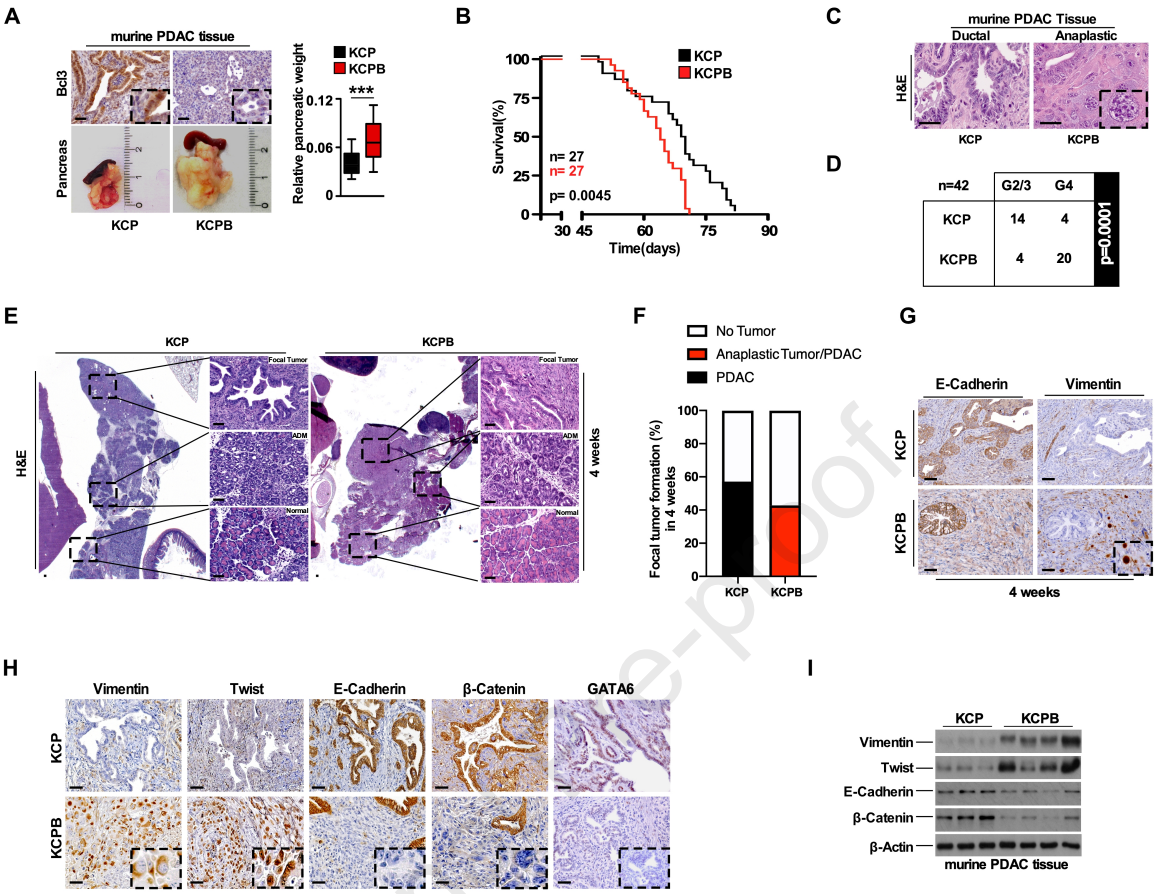

Figure 2

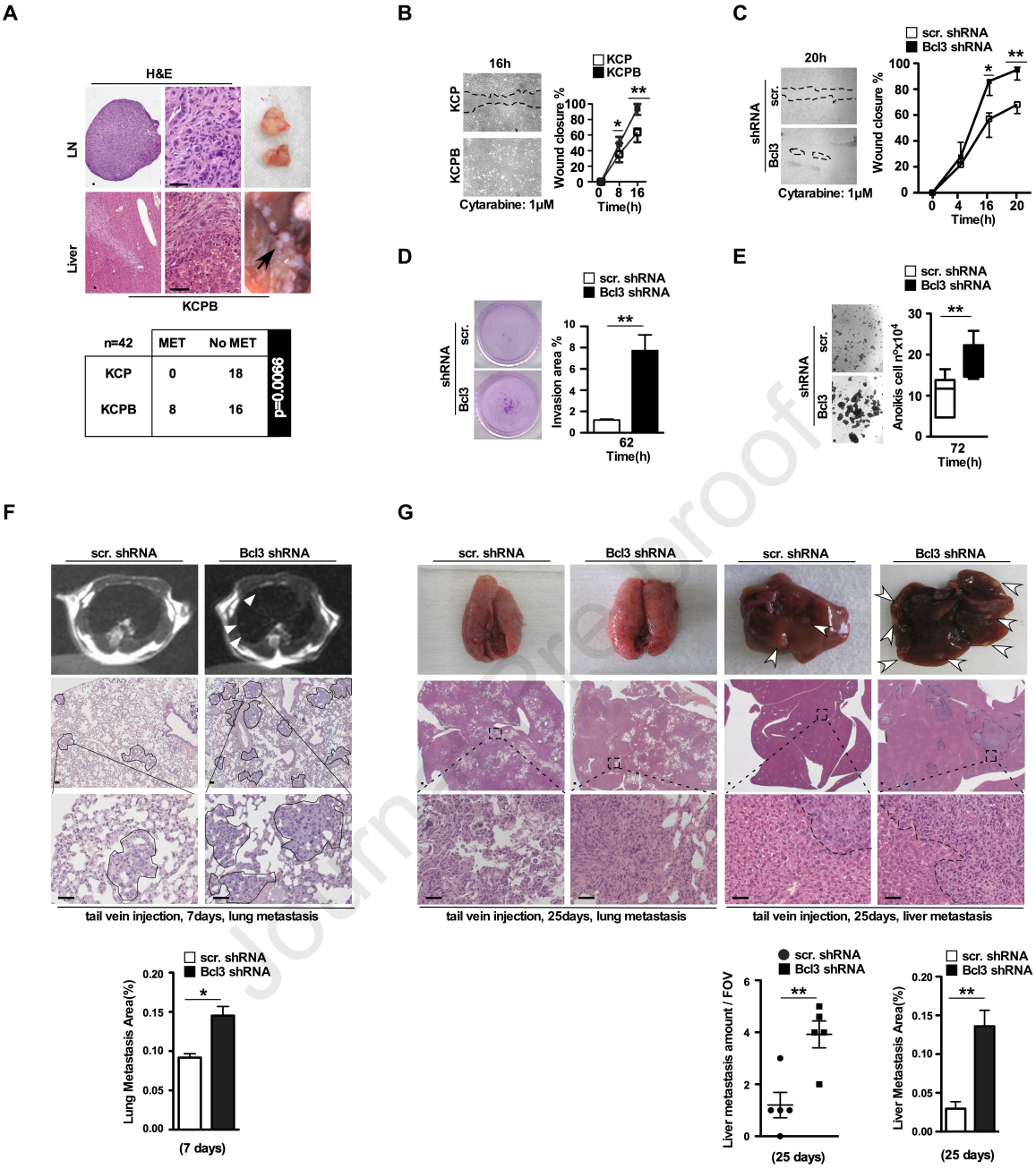
A
H&E
LN
Liver
KCPB
n=42
MET
No MET
KCP
0
18
KCPB
8
16
p=0.0066
B
16h
KCP
KCPB
KCP
KCPB
Wound closure %
Time(h)
Cytarabine: 1μM
C
20h
scr. shRNA
Bcl3 shRNA
shRNA
scr.
Bcl3
Wound closure %
Cytarabine: 1μM
Time(h)
D
scr. shRNA
Bcl3 shRNA
shRNA
scr.
Bcl3
Invasion area %
62
Time(h)
E
scr. shRNA
Bcl3 shRNA
shRNA
scr.
Bcl3
Anoikis cell n^x10^4
72
Time(h)
F
scr. shRNA
Bcl3 shRNA
tail vein injection, 7days, lung metastasis
Lung Metastasis Area(%)
(7 days)
G
scr. shRNA
Bcl3 shRNA
scr. shRNA
Bcl3 shRNA
tail vein injection, 25days, lung metastasis
tail vein injection, 25days, liver metastasis
Liver metastasis amount / FOV
(25 days)
Liver Metastasis Area(%)
(25 days)

Figure 3

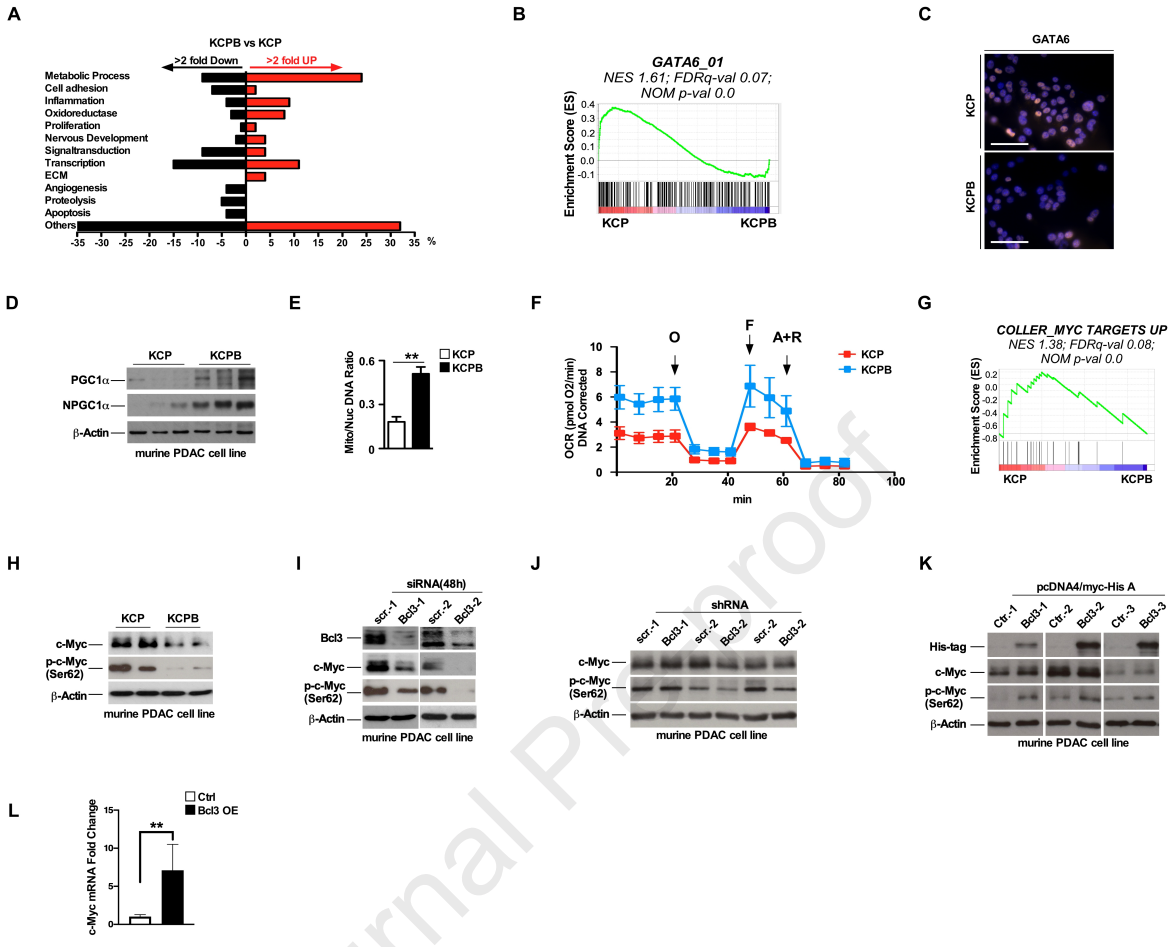

Figure 4

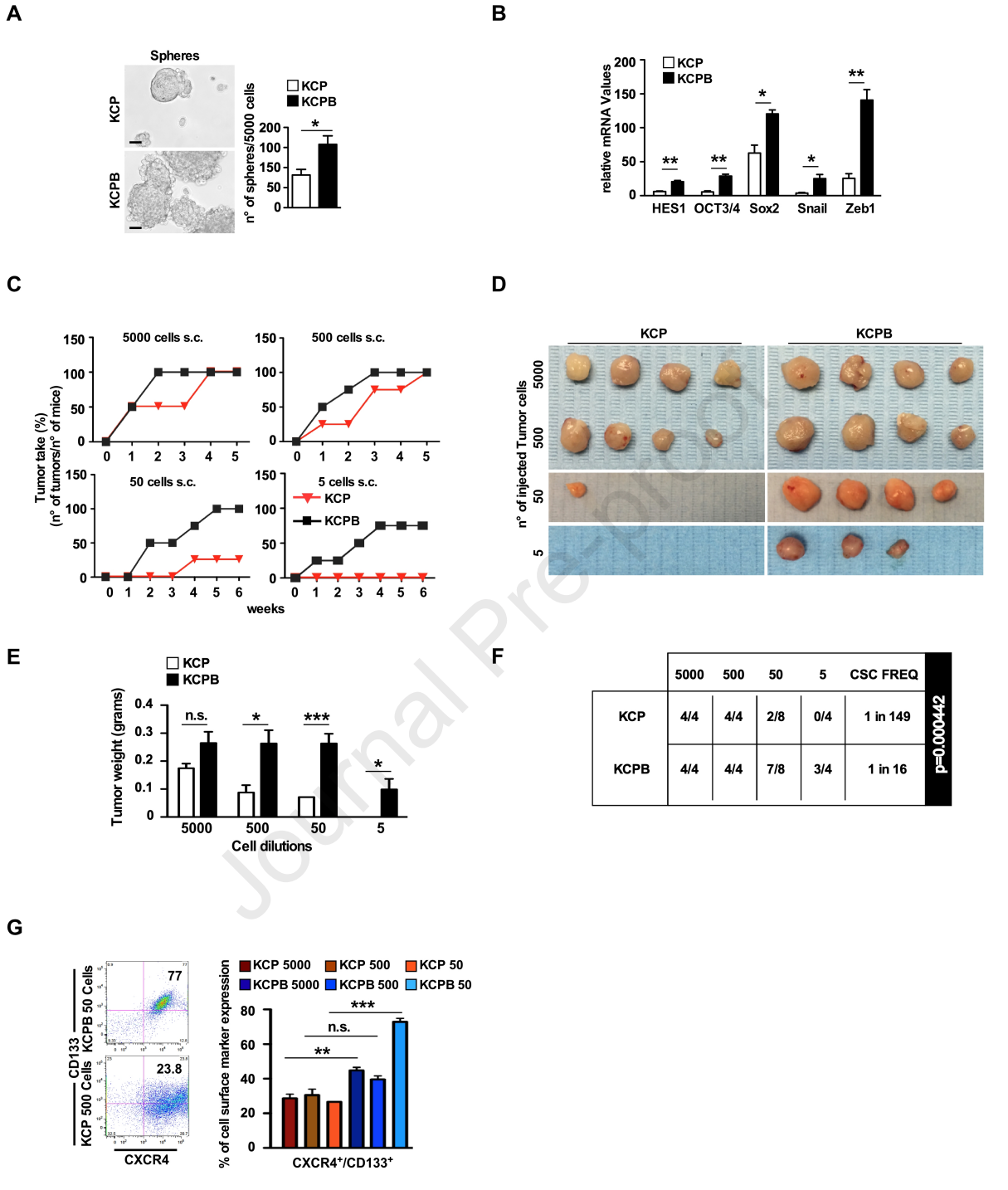
A
Spheres
KCP
KCPB
n° of spheres/5000 cells
B
relative mRNA Values
HES1
OCT3/4
Sox2
Snail
Zeb1
C
5000 cells s.c.
500 cells s.c.
50 cells s.c.
5 cells s.c.
Tumor take (%)
(n° of tumors/n° of mice)
weeks
D
n° of injected Tumor cells
E
Tumor weight (grams)
n.s.
Cell dilutions
F
5000
500
50
5
CSC FREQ
KCP
4/4
4/4
2/8
0/4
1 in 149
KCPB
4/4
4/4
7/8
3/4
1 in 16
p=0.000442
G
CD133
KCP 500 Cells
KCPB 50 Cells
77
23.8
CXCR4
KCP 5000
KCP 500
KCP 50
KCPB 5000
KCPB 500
KCPB 50
% of cell surface marker expression
CXCR4+/CD133+

Figure 5

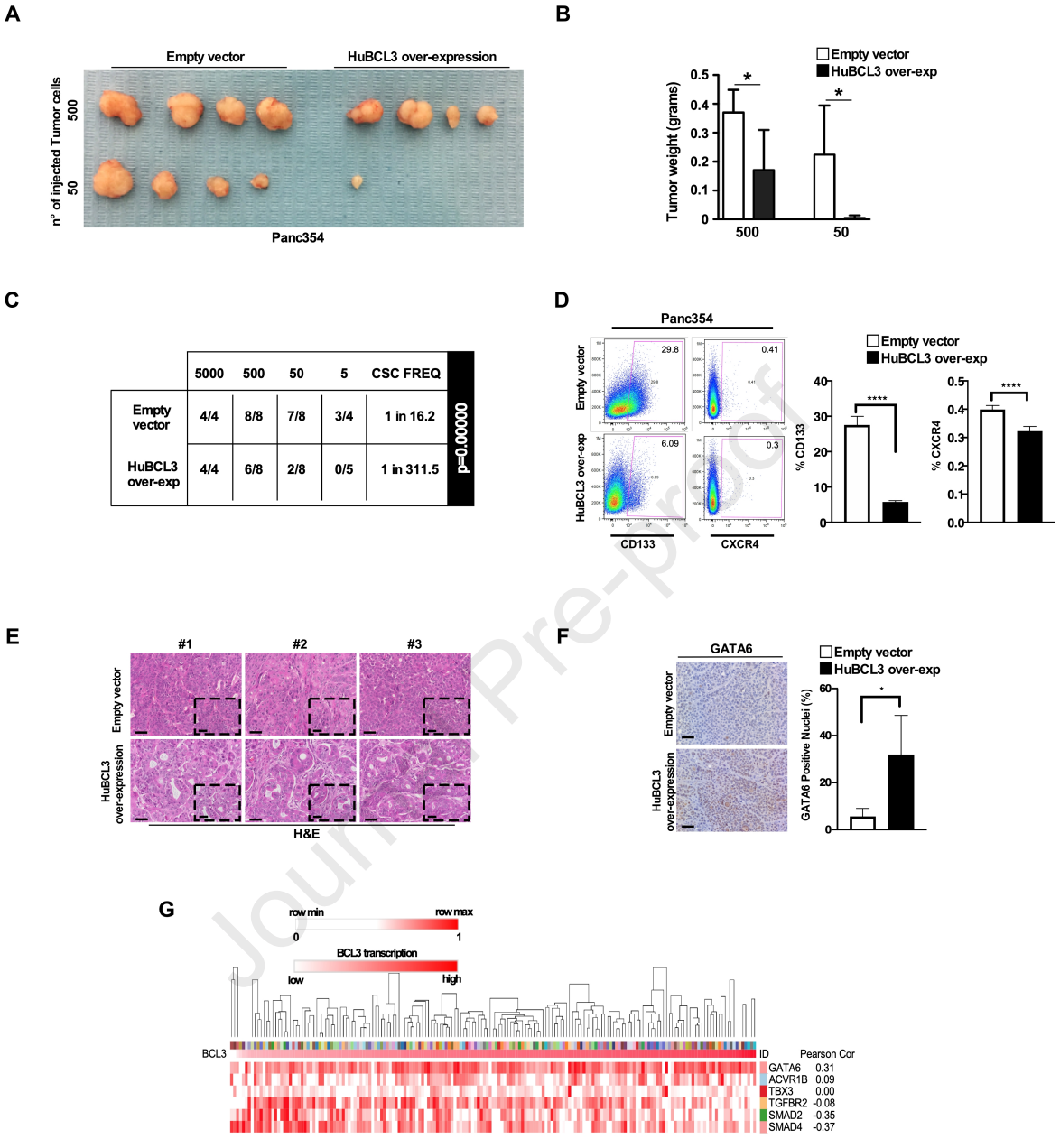

Figure 6

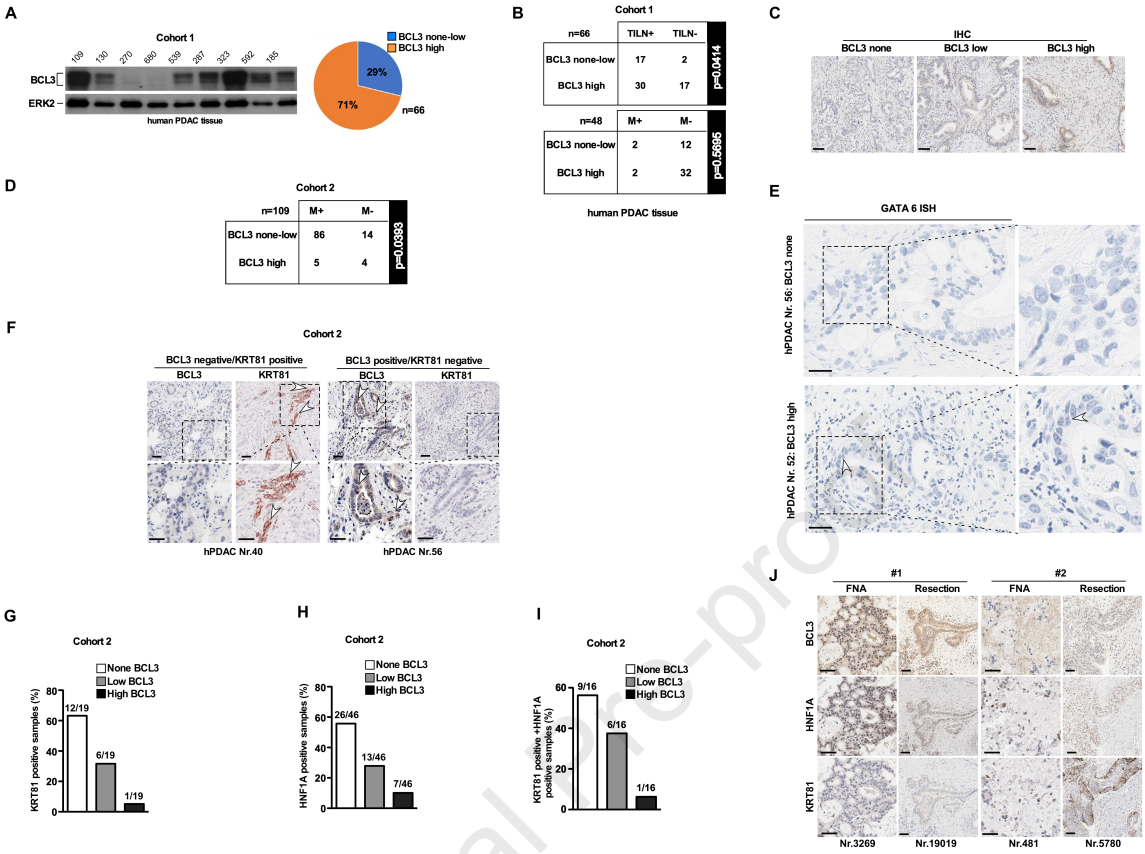

Figure 7

BACKGROUND AND CONTEXT

Efficient molecular subtyping of pancreatic ductal adenocarcinoma (PDAC) promises for a better understanding of PDAC biology and improved therapeutic approaches. Considering that the role of CSCs in molecular subtypes remains largely unknown, the authors analyzed the role of BCL3, an important NF-κB regulator, in CSC-ness and PDAC molecular subtypes.

NEW FINDINGS

The authors link BCL3 deficiency (1) to tumor aggressiveness *in vitro* and *in vivo* across species, (2) to the expansion of CSCs, and (3) to non-classical molecular PDAC subtypes.

LIMITATIONS

As a part of the NF-κB pathway, BCL3 deficiency exploits the pillars of CSC biology affecting pancreatic cancer aggressiveness. Further studies will be required to reveal the functions of each regulator of this pathway in PDAC CSC-ness and molecular subtypes.

IMPACT

BCL3 is presented in this study as a putative stratification marker for non-classical PDAC subtypes and tumor aggressiveness.